International Society for Rock Mechanics and Rock Engineering
Norwegian Group for Rock Mechanics

ISRM International Symposium
Eurock 2025 – Expanding the Underground Space
Trondheim, Norway, 16-20 June
ISBN 978-82-8208-079-8

On modelling quasi-static uniaxial tension and compression tests on rock with explicit time stepping

T. Saksala
Tampere University, Finland
timo.saksala@tuni.fi

Abstract

Modelling rock failure in engineering applications, such as blasting and percussive drilling, involve stress wave propagation, high stress rates, and substantial fracturing/fragmentation during extremely short time spans. Such circumstances dictate using explicit time stepping in solving the global system of problem governing equations.

The material model development requires validation under dynamic loadings, especially in uniaxial tension and compression tests. However, the failure model must also be able to predict the quasi-static uniaxial tensile and compressive strengths as well as the failure modes of the rock type involved. Unfortunately, the explicit time stepping is only conditionally stable and, thus, modelling quasi-static tests of a laboratory sample size numerical rock sample becomes a computationally laborious task. It is, therefore, tempting to increase the loading rate as much as possible when performing these validation simulations.

Notwithstanding, using too high strain rates leads to strain rate hardening effects and affect the failure mode, triggering even a transition from a single (few) macro-failure plane(s) to multiple fracture/fragmentation beyond certain loading rate depending on the loading type and sample size. However, there seems to be no guiding lines in the literature as to how high a loading rate can be used in uniaxial tension and compression tests, to save the CPU time, so that the simulation results can still be considered valid.

The present study addresses this gap of knowledge by performing a series of numerical tests on brittle rock under uniaxial tests using an explicit (in time) finite element code. The rock failure is described in the continuum sense based on a damage-viscoplasticity model. The 2D simulations demonstrate that with a sample of size 25×50 (mm), strain rates up to 1 s^{-1} can be used in both tension and compression without significant deviations from the quasi-static case.

Keywords

Uniaxial quasi-static tests, Strain rate, Explicit time integration, Rock failure

ISRM

NBG

1 Introduction

Rock failure prediction by numerical modelling is a routine task in rock engineering and geotechnical applications (Zhou and Zhao 2011; Zhang and Zhao 2014). This is particularly important under dynamic applications, such as blasting and percussive drilling, where transient loadings and highly deforming/fracturing geomaterials dictate the adoption of explicit time stepping schemes. Moreover, the discrete element method (DEM), and particle methods in general, is inherently explicit in time (Jing and Stephansson 2007; Potyondy and Cundall 2004). Unfortunately, explicit time stepping is only conditionally stable in time (Hughes 1987), which usually limit their usability to transient, short duration problems.

However, development of material models for fracturing rock under dynamic loading requires validation simulations also in quasi-static tests with loading ranges from 10^{-5} to 10^{-2} s^{-1} (Zhang and Zhao 2014). Now, because the stable time step, i.e. the Courant limit, of an explicit time marching depends on the finite element size and the wave speed (Hughes 1987), carrying out numerical quasi-static tests is practically unfeasible, especially in 3D. For this reason, the validation simulations of the explicit codes are usually carried out at elevated rates (e.g., at 0.5 s^{-1} in Huan et al. 2019), which, however, may invalidate the quasi-static nature of the simulations because rock is a highly strain-rate sensitive material (Zhang and Zhao 2014). A rate too high results in rate hardening and multiple macrofailure planes.

The question thus arises: what is the safe upper strain rate at which numerical uniaxial compression and tension tests can be carried out with results not deviating too much from the quasi-static ones? The present paper answers to this question by performing numerical simulations in 2D case with the continuum approach based on the finite element method and a damage-viscoplastic model for rock failure.

2 Numerical method

2.1 Rock failure model

The rock material is taken as isotropic and linear elastic until the uniaxial strength (elastic limit) is reached in both tension and compression. Upon reaching the elastic limits, nonlinear softening commences. The softening processes in both tension and compression are governed by separate scalar damage variables due to the asymmetry of rock behavior in these stress regimes. The rate sensitivity is accommodated by consistent viscoplasticy by Wang et al. (1997). Moreover, the small deformation framework is assumed. Within this setting then, stress states leading to inelastic strain and damage are indicated by the Mohr-Coulomb (MC) criterion for shear/compression and the Rankine (R) criterion as the tensile cut-off, mathematically written as

$$f_{\mathrm{MC}}(\overline{\boldsymbol{\sigma}}, \dot{\lambda}_{\mathrm{MC}}) = \frac{k_\varphi - 1}{2}(\sigma_x + \sigma_y) + (k_\varphi + 1)\sqrt{\left(\frac{\sigma_x - \sigma_y}{2}\right)^2 + \sigma_{xy}^2} - \sigma_c(\dot{\lambda}_{\mathrm{MC}}) \tag{1}$$

$$f_{\mathrm{R}}(\boldsymbol{\sigma}, \dot{\lambda}_{\mathrm{R}}) = \frac{\sigma_x + \sigma_y}{2} + \sqrt{\left(\frac{\sigma_x - \sigma_y}{2}\right)^2 + \sigma_{xy}^2} - \sigma_t(\dot{\lambda}_{\mathrm{R}}) \tag{2}$$

$$\sigma_c(\dot{\lambda}_{\mathrm{MC}}) = \sigma_{c0} + s_{\mathrm{MC}}\dot{\lambda}_{\mathrm{MC}}, \quad \sigma_t(\dot{\lambda}_{\mathrm{R}}) = \sigma_{t0} + s_{\mathrm{R}}\dot{\lambda}_{\mathrm{R}} \tag{3}$$

$$f_i \leq 0, \quad \dot{\lambda}_i \geq 0, \quad \dot{\lambda}_i f_i = 0 (i = \mathrm{MC}, \mathrm{R}) \tag{4}$$

The notations in these equations are as follows: $\overline{\boldsymbol{\sigma}}$ is the stress effective tensor with $\sigma_x, \sigma_y, \sigma_{xy}$ being its 2D components; $k_\varphi = (1 + \sin\varphi)/(1 - \sin\varphi)$ with φ being the internal friction angle; $\dot{\lambda}_{\mathrm{MC}}, \dot{\lambda}_{\mathrm{R}}$ are the viscoplastic multipliers, respectively; σ_{c0}, σ_{t0} are the quasi-static elasticity limits in compression and tension, respectively; $s_{\mathrm{MC}}, s_{\mathrm{R}}$ are the viscosity moduli in compression and tension, respectively. Eqs. (4) are the consistency conditions, which are imposed in the consistency approach similarly as in rate-independent plasticity (Wang et al. 1997).

The damage part of the model reads as

$$\omega_t(\varepsilon_{\mathrm{eqvt}}^{\mathrm{vp}}) = A_t\left(1 - \exp\left(-\beta_t \varepsilon_{\mathrm{eqvt}}^{\mathrm{vp}}\right)\right), \quad \omega_c(\varepsilon_{\mathrm{eqvc}}^{\mathrm{vp}}) = A_c\left(1 - \exp\left(-\beta_c \varepsilon_{\mathrm{eqvc}}^{\mathrm{vp}}\right)\right) \tag{5}$$

$$\dot{\varepsilon}_{\mathrm{eqvt}}^{\mathrm{vp}} = \sqrt{\textstyle\sum_{k=1}^{2} \langle \dot{\varepsilon}_{\mathrm{vp},k} \rangle}, \quad \dot{\varepsilon}_{\mathrm{eqvc}}^{\mathrm{vp}} = \sqrt{\frac{2}{3}\dot{\mathbf{e}}_{\mathrm{vp}} : \dot{\mathbf{e}}_{\mathrm{vp}}}, \; \dot{\mathbf{e}}_{\mathrm{vp}} = \dot{\boldsymbol{\varepsilon}}_{\mathrm{vp}} - \frac{1}{3}\mathrm{tr}(\dot{\boldsymbol{\varepsilon}}_{\mathrm{vp}}) \tag{6}$$

$$\dot{\boldsymbol{\varepsilon}}_{\mathrm{vp}} = \dot{\lambda}_{\mathrm{MC}} \frac{\partial f_{\mathrm{MC}}}{\partial \bar{\boldsymbol{\sigma}}} + \dot{\lambda}_{\mathrm{R}} \frac{\partial f_{\mathrm{R}}}{\partial \bar{\boldsymbol{\sigma}}} \tag{7}$$

where the symbol meanings are: ω_t, ω_c are the damage variables in tension and compression, respectively; A_t, A_c are parameters that control the final value of the damage variables, respectively; $\beta_t = \sigma_{\mathrm{t0}} h_e / G_{\mathrm{Ic}},\ \beta_c = \sigma_{\mathrm{c0}} h_e / G_{\mathrm{IIc}}$ are parameters control the initial slope and the amount of damage dissipation, being defined by the mode I, G_{Ic}, and II, G_{IIc}, fracture energies and h_{e} is a characteristic length of a finite element; $\varepsilon_{\mathrm{eqvt}}^{\mathrm{vp}}, \varepsilon_{\mathrm{eqvc}}^{\mathrm{vp}}$ are the equivalent viscoplastic strains driving the damage (they are the integrated forms of the rates $\dot{\varepsilon}_{\mathrm{eqvt}}^{\mathrm{vp}}$ and $\dot{\varepsilon}_{\mathrm{eqvc}}^{\mathrm{vp}}$; $\langle \cdot \rangle$ are the Macaulay brackets, i.e. the positive part operator; $\dot{\boldsymbol{\varepsilon}}_{\mathrm{vp}}, \dot{\mathbf{e}}_{\mathrm{vp}}$ are the rate of viscoplastic strain and its deviatoric part, respectively. Eq. (7) is the flow rule for bi-surface viscoplasticity.

As the damage is driven by viscoplastic strain only, this model does not need separate loading functions to indicate damaging. Moreover, the effective stress space formulation (Grassl and Jirasek 2006) is adopted whereby the plasticity and damage computations are separated so that, first, the stress stated violating the failure criteria (Eqs. (1) and (2)) is returned to the yield surface and then, the damage variables are updated by Equations (5). Finally, the nominal stress, $\boldsymbol{\sigma}$, is calculated by operating with the damage variables on the effective stress, $\bar{\boldsymbol{\sigma}}$, returned on the yield surface. The Lee and Fenves (Lee and Fenves 1998) relation is chosen for this end:

$$\boldsymbol{\sigma} = (1 - s_c \omega_t)(1 - s_t \omega_c)\bar{\boldsymbol{\sigma}},\ \ \bar{\boldsymbol{\sigma}} = \mathbf{E}\!:\!\left(\boldsymbol{\varepsilon} - \boldsymbol{\varepsilon}_{\mathrm{vp}}\right) \tag{8}$$

$$s_t = 1 - w_t r(\bar{\sigma}_i),\ \ s_c = 1 - w_c(1 - r(\bar{\sigma}_i)),\ \ 0 \le w_t, w_c \le 1 \tag{9}$$

$$r(\bar{\sigma}_i) = \textstyle\sum_{i=1}^{2} \langle \bar{\sigma}_i \rangle \big/ \sum_{i=1}^{2} |\bar{\sigma}_i| \tag{10}$$

where: s_t and s_c are stiffness recovery functions depending on the principal nominal stresses, $\bar{\sigma}_i$; Parameters w_t and w_c control the degree of recovery; $\mathbf{E}$ is the elasticity tensor. Unilateral nature of microcracking is neglected in this study because only monotonous loadings are considered. Thereby, $w_c = 0$ and $w_t = 0$, yielding $s_c = 1$ and $s_t = 1$.

Linearisation of the model is needed for quasi-static simulation of the uniaxial tests. The final result, i.e. the consistent tangent stiffness operator used in the Newton-Raphson iteration of the global equation of balance of linear momentum (Ottosen and Ristinmaa 2005), is given as (see Saksala 2022 for the derivation):

$$\mathbf{E}_{\mathrm{epd}} = \phi \mathbf{E} - \left(\phi \mathbf{E} + (1 - \omega_t)(\bar{\boldsymbol{\sigma}} \otimes \mathbf{C}_c) + (1 - \omega_c)(\bar{\boldsymbol{\sigma}} \otimes \mathbf{T}_d)\right) \cdot \mathbf{C}_p \tag{11}$$

$$\phi = (1 - \omega_t)(1 - \omega_c) \tag{12}$$

$$\mathbf{T}_d = \tfrac{1}{3}\beta_d A_d \exp\!\left(-\beta_d \varepsilon_{\mathrm{eqvt}}^{\mathrm{vp}}\right) \max\!\left(0, \mathrm{sgn}\!\left(\Delta\boldsymbol{\varepsilon}_{\mathrm{vp}} : \mathbf{1}\right)\right) \mathbf{1} \quad (\mathbf{1}_{ij} = \delta_{ij}) \tag{13}$$

$$\mathbf{C}_d = \tfrac{2}{3}\beta_c A_c \frac{\exp\!\left(-\beta_c \varepsilon_{\mathrm{eqvc}}^{\mathrm{vp}}\right)}{\varepsilon_{\mathrm{eqvc}}^{\mathrm{vp}}} \Delta\mathbf{e}_{\mathrm{vp}} \tag{14}$$

$$\mathbf{C}_p = \mathbf{T}_p^{-1} \cdot \mathbf{A}_p,\ \mathbf{T}_p = \left(\mathbb{I} + \left(\Delta\lambda_{\mathrm{R}} \frac{\partial^2 f_{\mathrm{R}}}{\partial \bar{\boldsymbol{\sigma}}^2} + \Delta\lambda_{\mathrm{MC}} \frac{\partial^2 f_{\mathrm{MC}}}{\partial \bar{\boldsymbol{\sigma}}^2}\right) : \mathbf{E}\right) \tag{15}$$

$$\mathbf{A}_p = \left(\Delta\lambda_{\mathrm{R}} \frac{\partial^2 f_{\mathrm{R}}}{\partial \bar{\boldsymbol{\sigma}}^2} + \Delta\lambda_{\mathrm{MC}} \frac{\partial^2 f_{\mathrm{MC}}}{\partial \bar{\boldsymbol{\sigma}}^2}\right) : \mathbf{E} + \frac{\partial f_{\mathrm{R}}}{\partial \bar{\boldsymbol{\sigma}}} \otimes \mathbf{F}_t + \frac{\partial f_{\mathrm{MC}}}{\partial \bar{\boldsymbol{\sigma}}} \otimes \mathbf{F}_c \tag{16}$$

$$\mathbf{F}_c = \tfrac{1}{|\mathbf{G}|}\left(G_{22} \tfrac{\partial f_{\mathrm{MC}}}{\partial \bar{\boldsymbol{\sigma}}} : \mathbf{E} - G_{12} \tfrac{\partial f_{\mathrm{R}}}{\partial \bar{\boldsymbol{\sigma}}} : \mathbf{E}\right),\ \ \mathbf{F}_t = \tfrac{1}{|\mathbf{G}|}\left(-G_{21} \tfrac{\partial f_{\mathrm{MC}}}{\partial \bar{\boldsymbol{\sigma}}} : \mathbf{E} + G_{11} \tfrac{\partial f_{\mathrm{R}}}{\partial \bar{\boldsymbol{\sigma}}} : \mathbf{E}\right) \tag{17}$$

$$\mathbf{G} = \begin{bmatrix} \frac{\partial f_{\mathrm{MC}}}{\partial \bar{\boldsymbol{\sigma}}} : \mathbf{C}_{\mathrm{e}} : \frac{\partial f_{\mathrm{MC}}}{\partial \bar{\boldsymbol{\sigma}}} + \frac{s_{\mathrm{MC}}}{\Delta t} & \frac{\partial f_{\mathrm{MC}}}{\partial \bar{\boldsymbol{\sigma}}} : \mathbf{C}_{\mathrm{e}} : \frac{\partial f_{\mathrm{R}}}{\partial \bar{\boldsymbol{\sigma}}} \\ \frac{\partial f_{\mathrm{R}}}{\partial \bar{\boldsymbol{\sigma}}} : \mathbf{C}_{\mathrm{e}} : \frac{\partial f_{\mathrm{MC}}}{\partial \bar{\boldsymbol{\sigma}}} & \frac{\partial f_{\mathrm{R}}}{\partial \bar{\boldsymbol{\sigma}}} : \mathbf{C}_{\mathrm{e}} : \frac{\partial f_{\mathrm{R}}}{\partial \bar{\boldsymbol{\sigma}}} + \frac{s_{\mathrm{R}}}{\Delta t} \end{bmatrix} \tag{18}$$

The symbol meanings are: $\mathbb{I}$ is the fourth order unit tensor, δ_{ij} is the Kronecker's delta, $\Delta\lambda_{\mathrm{R}}$, $\Delta\lambda_{\mathrm{MC}}$ and $\Delta\boldsymbol{\varepsilon}_{\mathrm{vp}}$, $\Delta\mathbf{e}_{\mathrm{vp}}$ are the viscoplastic increments and total and deviatoric strains, respectively, accumulated during the stress return mapping; G_{ij} are the entries of matrix $\mathbf{G}$ in Eq. (18). The first and second derivatives of the yield functions are directly obtained from Eqs. (1) and (2). Finally, Eqs. (13) and (14) originate from differentiation of damage functions (5).

2.2 Explicit time integration of the equations of motion

The finite element discretized global equations of motion, solved in dynamics, and its static version (obtained by setting the acceleration to zero) can be derived by standard steps (see, e.g., Ottosen and Ristinmaa 2005). When the modified Euler method (Hahn 1991) is employed as the explicit time integrator, the response of the system is solved by

$$\mathbf{M}\ddot{\mathbf{u}}_t + \mathbf{f}_t^{\mathrm{int}}(\mathbf{u}_t, \dot{\mathbf{u}}_t, \omega_{\mathrm{t}}, \omega_c) = \mathbf{f}_t^{\mathrm{ext}} \rightarrow \ddot{\mathbf{u}}_t \tag{19}$$

$$\dot{\mathbf{u}}_{t+\Delta t} = \dot{\mathbf{u}}_t + \Delta t \ddot{\mathbf{u}}_t \tag{20}$$

$$\mathbf{u}_{t+\Delta t} = \mathbf{u}_t + \Delta t \dot{\mathbf{u}}_{t+\Delta t} \tag{21}$$

$$\mathbf{f}_t^{\mathrm{int}} = \mathbf{A}_{e=1}^{\mathrm{N_{el}}} \int_{\Omega^{\mathrm{e}}} \mathbf{B}_{\mathrm{u}}^{\mathrm{e,T}} \boldsymbol{\sigma}(\mathbf{u}_t, \dot{\mathbf{u}}_t, \omega_{\mathrm{t}}, \omega_{\mathrm{c}}) \mathrm{d}\Omega \tag{22}$$

where $\mathbf{M}$ is the lumped mass matrix, $\mathbf{f}_t^{\mathrm{int}}$ is the internal force vector, $\mathbf{B}_{\mathrm{u}}^{\mathrm{e}}$ is the kinematic matrix containing the components of the gradient of the interpolation matrix $\mathbf{N}_{\mathrm{e}}$, $\mathbf{A}$ is the standard finite element assembly operator, $\mathbf{f}_t^{\mathrm{ext}}$ is the external force vector (not needed here), Δt is the time step, and $\mathbf{u}_t, \dot{\mathbf{u}}_t, \ddot{\mathbf{u}}_t$ are the displacement, velocity and acceleration vector, respectively. In the quasi-static case, the inertia term in Eq. (19) is dismissed and the internal force vector is linearized, which essentially results in the tangent operator in Eq. (11). The system is then solved iteratively by the Newton-Raphson scheme. The stable time step for explicit simulations is estimated by

$$\Delta t = \frac{2\pi}{k \cdot \max(\sqrt{K_{ii}/M_{ii}})} \tag{24}$$

where K_{ii} and M_{ii} are the diagonal entries of the (elastic) stiffness matrix and the lumped mass matrix for the smallest element in the mesh, and k is a correction coefficient.

3 Numerical examples

3.1 Material properties and model parameter values

The material and model parameters for the rock-like material used in simulations are given in Table 1.

Table 1. Material properties and model parameters values for simulations.

Parameter/Material property	**Value and unit**
Young's modulus (E)	60 GPa
Poisson's ratio (ν)	0.25
Density (ρ)	2600 kg/m^3
Compressive strength (σ_{c0})	100 MPa
Tensile strength (σ_{t0})	10 MPa
Mode I fracture energy (G_{Ic})	100 N/m
Mode II fracture energy (G_{IIc})	2000 N/m
Internal friction angle (φ)	50 °
Viscosity modulus in tension (s_R)	0.01 MPa·s
Viscosity modulus in compression (s_{MC})	0.01 MPa·s
Maximum tensile damage (A_t)	0.98
Maximum compressive damage (A_c)	0.98

Whether these values represent exactly any real rock is irrelevant because the purpose of the simulations is to compare the explicit method, at different strain rates, to the implicit one. In order to trigger the localization of deformation, i.e. failure mode of the numerical sample, naturally, the strength of each finite element is perturbed by adding a uniformly distributed random component to its tensile and compressive strength. More specifically, the tensile and compressive strength distribution in the mesh is uniformly distributed between 9 and 11 MPa and 90 and 110 MPa, respectively. The finite element mesh and the strength distributions are shown in Fig. 1.

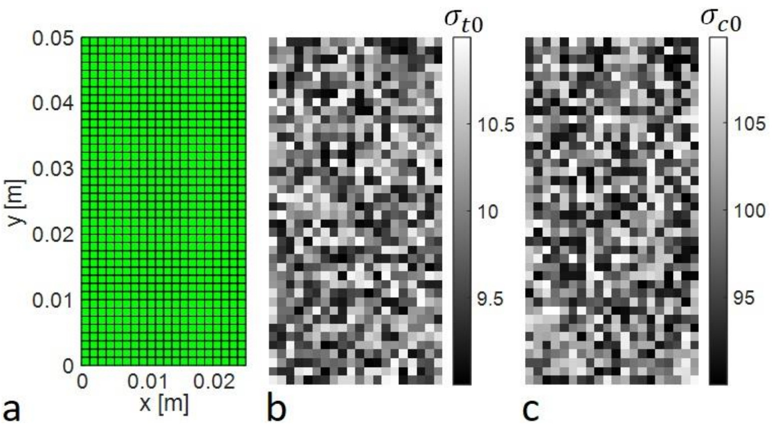

Fig. 1 (a) Finite element mesh (800 4-node quadrilateral elements); (b) Tensile strength distribution (MPa); Compressive strength distribution (MPa).

The 4-node (bilinear) quadrilateral element is chosen for the simulations. The boundary conditions are imposed on the top and bottom edges of the numerical sample so that the bottom is fixed, and the top is moving at constant velocity.

3.2 Uniaxial tension test

The uniaxial tension tests are first carried out on the numerical rock in Fig. 1. The relevant simulation results are shown in Fig. 2. The tensile damage distribution represents the average of its values at the four integration points of each element.

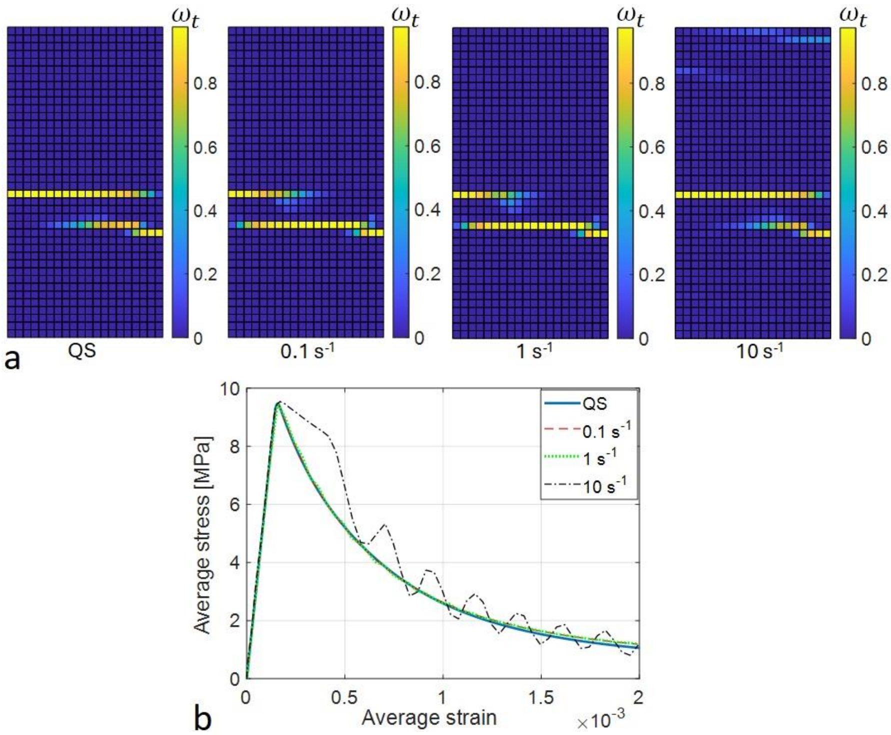

Fig. 2 Simulation results for uniaxial tension test: (a) Failure mode in terms of tensile damage distribution at different strain rates (QS = quasi-static); (b) Corresponding average stress-strain curves.

The failure mode predicted is the experimental transverse splitting of the sample, with a double crack system in each case. Interestingly, the failure mode predicted in the quasi-static case is replicated only at the highest tested strain rate 10 s^{-1}. At strain rates 0.1 and 1 s$^{-1,}$ the explicit solution exhibit two cracks, as in the quasi-static case, but it is the upper crack does not propagate as far as in the quasi-static case. However, the lower crack propagates much further, preventing the propagation of the upper crack, at the lower strain rates. At 10 s^{-1}, secondary cracking starts to appear, and the stress-strain response display substantial fluctuations. On the other hand, the compressive strength overshoot is not significant.

3.3 Uniaxial compression test

Uniaxial compression tests are finally performed with the relevant simulation results shown in Fig. 3.

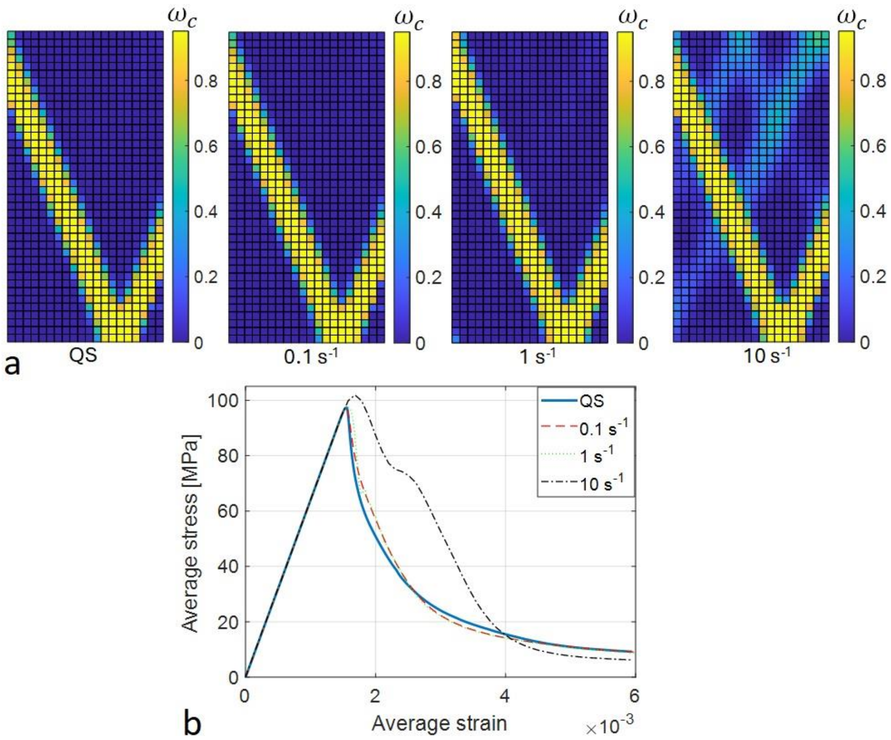

Fig. 3 Simulation results for uniaxial compression test: (a) Failure mode in terms of compressive damage distribution at different strain rates (QS = quasi-static); (b) Corresponding average stress-strain curves.

In contrast to tension, the predicted failure modes, attesting the experimentally witnessed "shearing along single plane" (Basu et al. 2013), are identical, upon eye inspection, in compression, as observed in Fig. 3a. However, some secondary cracking occurs again at 10 s^{-1}. Moreover, at this highest rate, the stress-strain response shows slight overshooting of compressive strength as well as more ductile post-peak response. At the lower strain rates, the responses from the explicit simulations deviate insignificantly from the quasi-static one.

4 Conclusions

This paper presented a numerical study comparing the quasi-static simulation of uniaxial tension and compression tests to the dynamic ones using explicit time integration. The finite element method-based continuum approach was adopted where the rock failure was described by a damage-viscoplastic model. The simulations demonstrated that, with the explicit time integration, strain rates up to 1 s^{-1} can be used without significant deviations from the quasi-static case in terms of failure modes and strengths in tension and compression. Furthermore, at lower strain rates, the explicit dynamics approach may predict failure modes with details differing from both the quasi-static and higher strain rate cases. This anomaly, demonstrated here in uniaxial tension simulations, merits more research in future. Finally, a full-blown 3D study should also be carried out.

References

Zhou Y, Zhao J (2011) Advances in rock dynamics and applications. CRC Press, Boca Raton. https://doi.org/10.1201/b11077

Zhang QB, Zhao J (2014) A Review of Dynamic Experimental Techniques and Mechanical Behaviour of Rock Materials. Rock Mechanics and Rock Engineering 47:1411-1478.

Jing L, Stephansson O (2007) Fundamentals of discrete element methods for rock engineering: Theory and Applications. Elsevier, New York. https://doi.org/10.1016/S0165-1250(07)85001-2

Potyondy DO, Cundall PA (2004) A bonded-particle model for rock. International Journal of Rock Mechanics and Mining Sciences. 41(8):1329-1364.

Hughes TJR (1987) The Finite Element Method: Linear Static and Dynamic Finite Element analysis, Prentice-Hall, Englewood Cliffs, NJ.

Huan Li, Yang J, Han Y, Yang C, Daemen JJK, Li P (2019) Weibull grain-based model (W-GBM) for simulating heterogeneous mechanical characteristics of salt rock. Engineering Analysis with Boundary Elements. 108:227-243.

Wang WM, Sluys LJ, De Borst R (1997) Viscoplasticity for instabilities due to strain softening and strain-rate softening. International Journal for Numerical Methods in Engineering. 40:3839–3864.

Grassl P, Jirásek M (2006) Damage-Plastic model for concrete failure. International Journal of Solids and Structures. 43:7166-7196.

Lee J, Fenves GL (1998) Plastic-damage model for cyclic loading of concrete structures. Journal of Engineering Mechanics. 124:892-900.

Ottosen NS, Ristinmaa M (2005) The Mechanics of Constitutive Modeling, Elsevier: Amsterdam.

Saksala T (2022) 3D numerical prediction of thermal weakening effects on granite. International Journal for Numerical and Analytical Methods in Geomechanics. 46:2770–2791.

Hahn GD (1991) A Modified Euler Method for dynamical analyses. International Journal for Numerical Methods in Engineering. 32:943- 955.

Basu A, Mishra DA, Roychowdhury K (2013) Rock failure modes under uniaxial compression, Brazilian, and point load tests. Bulletin of Engineering Geology and the Environment. 72:457–475.